Journal of Organometallic Chemistry 693 (2008) 2299–2309

Contents lists available at ScienceDirect

Journal of Organometallic Chemistry

journal homepage: www.elsevier.com/locate/jorganchem

Cytotoxic half-sandwich rhodium(III) complexes: Polypyridyl ligand influence on their DNA binding properties and cellular uptake

Michael A. Scharwitz [a], Ingo Ott [b], Yvonne Geldmacher [a], Ronald Gust [b], William S. Sheldrick [a,*]

[a] Lehrstuhl für Analytische Chemie, Ruhr-Universität Bochum, Universitätsstrasse 150, D-44780 Bochum, Germany
[b] Institut für Pharmazie, Freie Universität Berlin, Königin-Luise-Straße 2-4, D-14195 Berlin, Germany

ARTICLE INFO

Article history:
Received 12 February 2008
Received in revised form 1 April 2008
Accepted 2 April 2008
Available online 6 April 2008

Keywords:
Bioorganometallic chemistry
Rhodium
Polypyridyl ligands
DNA binding
Cytotoxicity
Cellular uptake

ABSTRACT

The DNA binding of polypyridyl (pp) $(\eta^5\text{-}C_5Me_5)Rh^{III}$ complexes of the types $[(\eta^5\text{-}C_5Me_5)RhCl(pp)](CF_3SO_3)$ (**2**–**6**) (pp = bpy, phen, dpq, dppz, dppn), $[(\eta^5\text{-}C_5Me_5)Rh\{(Me_2N)_2CS\}(pp)](CF_3SO_3)_2$ (**7**–**9**) (pp = dpq, dppz, dppn) and $[(\eta^5\text{-}C_5Me_5)Rh(L)(pp)](CF_3SO_3)$ (**10**) ($L = C_6H_5S^-$) and (**11**) ($L = C_{10}H_7S^-$) has been studied by UV/Vis spectroscopy, circular dichroismus and viscosity measurements. Complexes **3**–**11** are cytotoxic towards the human MCF-7 breast and HT-29 colon cancer cell lines and exhibit IC_{50} values in the range 0.56–10.7 μM. Stable intercalative binding into CT-DNA is indicated for the dpq and dppz complexes by large increases ΔT_m of 6–12 °C in the DNA thermal denaturation temperature for r = [complex]/[DNA] = 0.1 and by induced CD bands and large viscosity increases. In contrast, significant DNA lengthening is not observed after incubation of the biopolymer with the dppn complexes **2** and **9** at molar ratios of $r < 0.08$. Pronounced hypochromic shifts for the π–π^* transitions of the dppn ligands in the range 320–425 nm indicate the possible presence of surface stacking. The in vitro cytotoxicities of the chloro complexes **4**–**6** and the $(Me_2N)_2CS$ complexes **7**–**9** are dependent on the size of the polypyridyl ligand with IC_{50} values decreasing in the order dpq > dppz > dppn. For instance, IC_{50} values of 5.3, 1.5 and 0.91 μM were determined for **7**–**9** against MCF-7 cells. Rapid Cl^-/H_2O exchange leads the formation of aqua dications for **4**–**6**, whose levels of cellular uptake and cytotoxicities are similar to those established for **7**–**9**. Intramolecular interactions between the aromatic thiolate and dppz ligands of **10** and **11** prevent significant DNA intercalation. X-ray structural determinations have been performed for **2**–**7** and **11**.

1. Introduction

Organometallic compounds containing the Group 8 elements iron and ruthenium are attracting considerable current interest as potential anticancer agents [1–3]. For instance, ferrocifen, a ferrocenyl derivative of tamoxifen, exhibits promising antitumour activity and is a possible candidate for clinical trials [4]. Half-sandwich $(\eta^6\text{-arene})Ru^{II}$ complexes with imidazole [5], sulfoxide [6–8], phosphane [3,9], chelating amino acidato [10], and diamine or diimine ligands [2,11] have also been evaluated for cytotoxic activity. Such studies have recently been extended to analogous $(\eta^6\text{-arene})Os^{II}$ compounds [12–14].

Both the size of the arene and the lability of the Ru–Cl bond have found to play a crucial role in determining the cytotoxicity of ruthenium(II) complexes of the type $[(\eta^6\text{-arene})RuCl(LL')](PF_6)$ with bidentate ligands LL′. Compounds with extended polycyclic arenes (e.g. tetrahydroanthracene) and LL′ = ethylenediamine (en) are most active towards A2780 human ovarian cancer cells, whereas those with polar substituents on the arene or with aromatic diimine ligands such as 2,2′-bipyridine (bpy) or 1,10-phenanthroline (phen), exhibit either poor or no activity [2]. Further increases in the size of the polypyridyl ligand (pp) lead, however, to a dramatic reversal of the latter trend and the in vitro cytotoxicities of the complexes $[(\eta^6\text{-}C_6Me_6)RuCl(pp)](CF_3SO_3)$ towards the human cell lines HT-29 (colon cancer) and MCF-7 (breast cancer) are strongly dependent on the surface area of the aromatic system [15]. For instance, the IC_{50} values decreases from 11.1 over 2.12 to 0.13 μM for MCF-7 cells as the size of the polypyridyl ligand increases in the order dpq < dppz < dppn (dpq = dipyrido-[3,2-*f*:2′,3′-*h*]quinoxaline; dppz = dipyrido[3,2-*a*:2′,3′-*c*]phenazine; dppn = benzo[*i*]dipyrido[3,2-*a*:2′,3′-*c*]phenazine). These values correlate well with the cellular uptake efficiency, which increases from 1.1 over 146.6 to 906.7 ng(Ru)/mg(protein) within the series [15]. The kinetically inert complexes $[(\eta^6\text{-}C_6Me_6)Ru\{(NH_2)_2CS\}(pp)](CF_3SO_3)_2$ (pp = dppz, dppn) are also cytotoxic and this suggests that specific properties of the large polypyridyl ligands (e.g. DNA intercalation [16,17] and/or cleavage [18]) may be responsible for their biological activity. DNA binding studies indicate that $(\eta^6\text{-}C_6Me_6)Ru^{II}$ compounds containing dpq or particularly dppz

* Corresponding author. Tel.: +49 234 3224192; fax: +49 234 3214420.
E-mail address: william.sheldrick@rub.de (W.S. Sheldrick).

0022-328X/$ - see front matter © 2008 Elsevier B.V. All rights reserved.
doi:10.1016/j.jorganchem.2008.04.002

ligands are good metallointercalators but that the dppn ligand is too large to support stable intercalation between the base pairs of the double helix [15].

In striking contrast to their Group 8 neighbours, half-sandwich complexes of the Group 9 transition metals rhodium(III) and iridium(III) have attracted little interest as potential anticancer agents. An in vitro evaluation of the RAPTA analogues $[(\eta^6\text{-}p\text{-cymene})RhCl_2(pta)]$, $[(\eta^5\text{-}C_5Me_5)RhCl_2(pta)]$ and $[(\eta^5\text{-}C_5Me_5)RhCl(pta)_2]Cl$ (pta = 1,3,5-triaza-7-phosphatricyclo[3.3.1.1]decane) towards HT-29, A549 (lung carcinoma) and T47D (breast carcinoma) cells has recently been appeared [14], but the reported high IC_{50} values ($\geqslant$380 μM) are indicative of very limited cytotoxicity. In contrast, much lower IC_{50} values of, respectively, 7.4 and 0.41 μM have recently reported [15] for the $[(\eta^5\text{-}C_5Me_5)Ir^{III}$ complexes $[(\eta^5\text{-}C_5Me_5)IrCl(dppz)](CF_3SO_3)$ and $[(\eta^5\text{-}C_5Me_5)Ir\{(Me_2N)_2CS\}(dppn)](CF_3SO_3)_2$ [19] towards HT-29 cells. Interestingly, the increased lability of the Ir–Cl bond in the former complex leads to thermodynamically favoured coordinative Ir–N (nucleobase) binding to DNA rather than intercalation, as observed for the analogous $(\eta^6\text{-}C_6Me_6)Ru^{II}$ complex [15]. We now report DNA binding studies and evaluations of the in vitro cytotoxicity of polypyridyl half-sandwich Rh^{III} complexes of the types $[(\eta^5\text{-}C_5Me_5)RhCl(pp)](CF_3SO_3)$ (Scheme 1), $[(\eta^5\text{-}C_5Me_5)Rh\{(Me_2N)_2CS\}(pp)](CF_3SO_3)_2$ (pp = dpq, dppz, dppn) (Scheme 2) and $[(\eta^5\text{-}C_5Me_5)Rh(L)(dppz)](CF_3SO_3)$ (L = $C_6H_5S^-$, $C_{10}H_7S^-$) (Scheme 3). Two factors may be expected to possibly modify the biological properties of such Rh^{III} compounds with respect to analogous half-sandwich Ir^{III} or Ru^{II} complexes: (a) the increase in the rate of chloride substitution in the order $(\eta^6\text{-}C_6Me_6)Ru^{II} \ll (\eta^5\text{-}C_5Me_5)Ir^{III} < (\eta^5\text{-}C_5Me_5)Rh^{III}$ [20] and (b) the pronounced softness of the third-row transition metal Ir^{III} in comparison to Ru^{II} or Rh^{III}, owing to relativistic destabilisation of its 5d shell [21].

2. Results and discussion

2.1. Synthesis of *1*–*11*

The compounds of the type $[(\eta^5\text{-}C_5Me_5)RhCl(en)](CF_3SO_3)$ (**1**) and $[(\eta^5\text{-}C_5Me_5)RhCl(pp)](CF_3SO_3)$ (**2**–**6**) (pp = bpy, phen, dpq, dppz, dppn) were synthesised by heating the solvent complex $[(\eta^5\text{-}C_5Me_5)RhCl(acetone)_2](CF_3SO_3)$ with the appropriate polypyridyl ligand (pp) at 75 °C in CH_3OH/CH_2Cl_2 for 2 h. $[(\eta^5\text{-}C_5Me_5)RhCl(acetone)_2]^+$ was prepared in situ by addition of two equivalents of $Ag(CF_3SO_3)$ to a solution of the dinuclear starting compound $[\{(\eta^5\text{-}C_5Me_5)RhCl\}_2(\mu\text{-}Cl)_2]$ in acetone and subsequent filtration of precipitated AgCl after stirring in the dark for 0.5 h. Following removal of the remaining chloride by analogous treatment of complexes **4**–**6** with an equivalent of $Ag(CF_3SO_3)$ in acetone, addition of tetramethyl thiourea $(Me_2N)_2CS$ to the resulting in situ complex

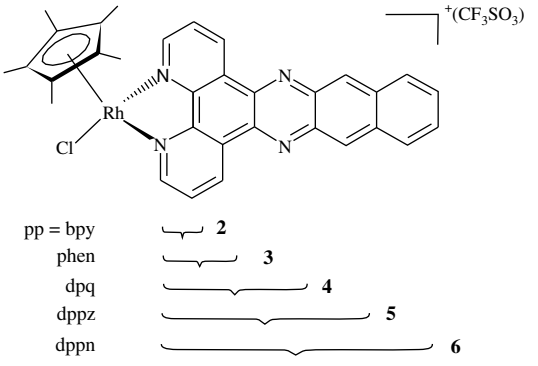

Scheme 1. Structures of complexes **2**–**6**.

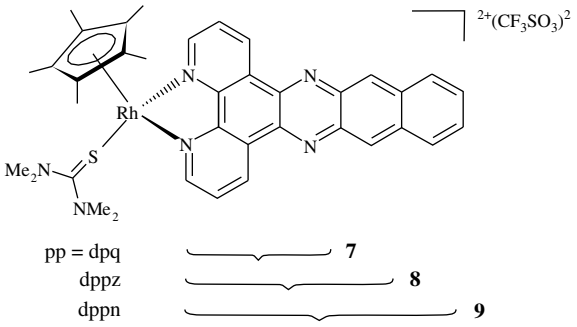

Scheme 2. Structures of complexes **7**–**9**.

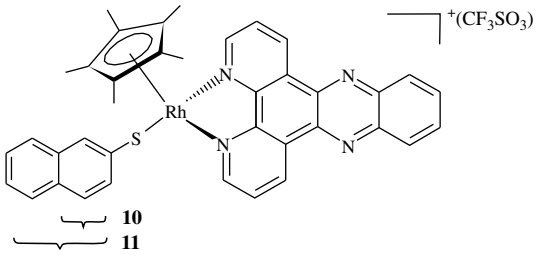

Scheme 3. Structures of complexes **10** and **11**.

$[(\eta^5\text{-}C_5Me_5)Rh(acetone)(pp)]^{2+}$ afforded $[(\eta^5\text{-}C_5Me_5)Rh\{(Me_2N)_2CS\}(pp)](CF_3SO_3)_2$ (**7**–**9**) (pp = dpq, dppz, dppn), after heating the reaction mixture for 2 h at 75 °C in CH_3OH/CH_2Cl_2. The dppz complexes $[(\eta^5\text{-}C_5Me_5)Rh(L)(dppz)](CF_3SO_3)$ (**10**) (L = $C_6H_5S^-$) and (**11**) (L = $C_{10}H_7S^-$) were prepared in an analogous manner by reaction of $[(\eta^5\text{-}C_5Me_5)Rh(acetone)(dppz)]^{2+}$ with solutions of the respective thiols C_6H_5SH and $C_{10}H_7SH$ in the presence of an equivalent of 30% $NaOH/CH_3OH$. All the complexes were characterised by ^1H and ^{13}C NMR and positve-ion LSIMS and gave satisfactory microanalyses. The molecular structures of **2**–**7** and **11** were determined by X-ray structural analysis (Table 1).

Complexes **1**–**3** (pp = en, bpy, phen) were synthesised for the purpose of evaluating their in vitro cytotoxicities towards the human cell lines MCF-7 and HT-29. Their cations have been previously characterised in the presence of other counter anions (**1**, Cl^- [22]; **2**, Cl^- [23–25], ClO_4^- [25]; **3**, Cl^- [23–25], ClO_4^- [25]) as has that of the dppz complex **5** (PF_6^- [26]), which itself is known [27]. Crystal structures have been reported for $[(\eta^5\text{-}C_5Me_5)RhCl(bpy)](ClO_4)$ [20] and $[(\eta^5\text{-}C_5Me_5)RhCl(phen)](ClO_4)$ [25]. The bond lengths and angles in the cations of **2** and **3** are similar to those determined for the same cations in the presence of perchlorate anions. For instance, complex **3** (pp = phen) exhibits Rh–N distances of 2.100 (2) and 2.121 (2) Å, Rh–C distances in the range 2.141 (3)–2.171 (3) and an Rh–Cl bond length of 2.406 (1) Å. The analogous distances in $[(\eta^5\text{-}C_5Me_5)RhCl(phen)](ClO_4)$ [25] are 2.109 (3) Å and 2.128 (3), 2.132 (5)–2.165 (4) and 2.386 (1) Å. Similar bond lengths are observed in complexes **4**–**6**, whose cations are depicted in Fig. 1. These exhibit C_s crystallographic symmetry in the cases of **4** and **6**. An interesting feature of the half-sandwich cations is the variability of the interplanar angle between their cyclopentadienyl and polypyridyl ring systems. Respective values of 76.6(2)°, 58.5(3)° and 71.6(5)° are found in complexes **4**–**6**. The significantly larger interplanar angles for **4** and **6** result from the adoption of a pronounced envelope conformation by the central five-membered NRhNCC chelate ring in these complexes (Fig. 1a and c). A measure of this distortion is given by the respective interplanar angles of 14.7(4)° in **4** and 9.6(2)° in **6** between the N1–Rh1–N1A and N1–C–C–N1A planes. In contrast,

Table 1
Crystal and refinement data for **2**–**6**, **7** and **11**

Compound	**2**	**3**	**4**	**5**	**6**	**7** · H_2O	**11** · $2H_2O$
M (g mol^{-1})	578.8	602.9	654.9	705.0	755.0	918.8	864.8
T (K)	294	294	113	163	103	294	100
Radiation	Mo Kα	Mo Kα	Mo Kα	Mo Kα	Cu Kα	Mo Kα	Mo Kα
Crystal system	Orthorhombic	Triclinic	Monoclinic	Triclinic	Monoclinic	Monoclinic	Monoclinic
space group	$Pmn2_1$	$P(-1)$	$P2_1/m$	$P(-1)$	$P2_1/m$	$P2_1/n$	$C2/c$
a (Å)	13.103(2)	7.963(1)	7.792(1)	8.166(2)	12.198(1)	8.787(2)	36.700(9)
b (Å)	8.461(1)	11.761(1)	12.166(1)	11.848(4)	12.396(1)	37.540(8)	8.787(2)
c (Å)	10.647(6)	13.099(2)	13.849(1)	15.698(4)	12.245(1)	12.292(3)	23.019(6)
α (°)	90	90.12(1)	90	73.42(3)	90	90	90
β (°)	90	99.56(2)	103.42(1)	76.09(2)	110.33(1)	97.63(3)	91.28(2)
γ (°)	90	98.26(2)	90	74.11(2)	90	90	90
V (Å^3)	1180.4(7)	1196.8(3)	1277.0(1)	1378.1(6)	1736.2(3)	4018.9(14)	7422(3)
Z	2	2	2	2	2	4	8
D (g cm^{-3})	1.629	1.673	1.703	1.699	1.444	1.518	1.548
F(000)	584	608	660	712	764	1872	3536
μ (mm^{-1})	0.974	0.964	0.913	0.853	5.713	0.659	0.638
$2\theta_{max}$ (°)	50	55	55	50.5	117.9	50	51.8
Collected reflections	1561	6626	8234	11544	6631	8822	33444
Independent reflections	1258	5467	3002	4892	2372	7081	7123
Refined parameters	160	313	211	384	245	426	500
R_1 [$I > 2\sigma(I)$]	0.048	0.032	0.047	0.045	0.056	0.122	0.054
wR_2 (all data)[a]	0.130	0.082	0.110	0.091	0.157	0.323	0.134
S (Goodness-of-fit)	1.117	1.042	1.058	0.648	1.057	0.957	0.845
Maximum/minimum Δp (e Å^{-3})	1.28/−0.54	0.49/−0.45	1.51/−0.54	0.50/−0.46	0.72/−0.65	0.97/−0.94	1.84/−0.80

[a] $wR_2 = [\sum w(F^2_o - F^2_c)^2 / \sum w(F^2_o)^2]^{1/2}$.

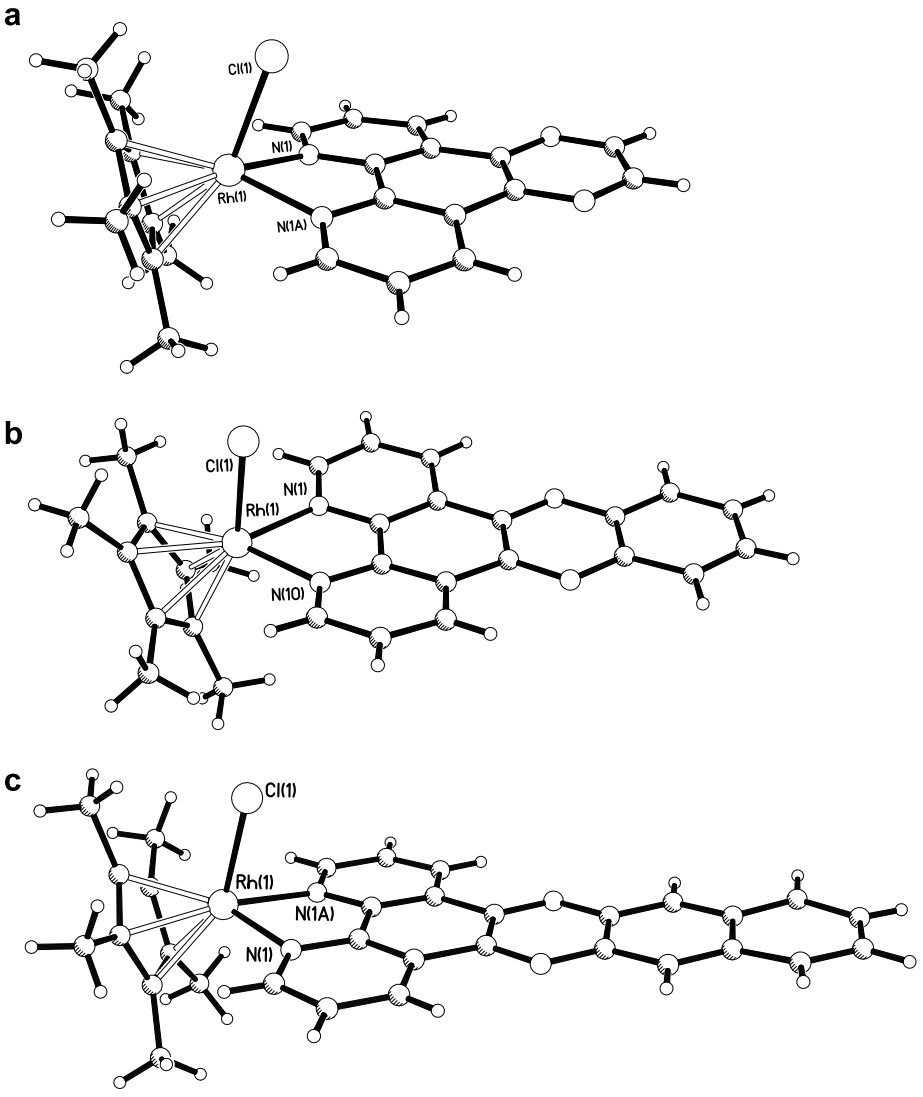

Fig. 1. Molecular structures of the cations of: (a) [(η^5-C_5Me_5)RhCl(dpq)](CF_3SO_3) (**4**), (b) [(η^5-C_5Me_5)RhCl(dppz)](CF_3SO_3) (**5**) and (c) [(η^5-C_5Me_5)RhCl(dppn)](CF_3SO_3) (**6**).

the chelate ring in the dppz complex **5** is almost flat with an analogous interplanar angle of only 1.7(5)°.

2.2. DNA binding studies

2.2.1. UV/Vis absorption and melting temperature measurements

Thermal denaturation measurements for calf thymus DNA (CT DNA) in the presence of transition metal complexes such as **1**–**11** can provide a simple means of gauging the strength of polypyridyl intercalation, provided that electrostatic and hydrogen bonding interactions remain effectively unchanged by pp ligand variation [27–29]. The ΔT_m values listed in Table 2 were recorded under equilibrium conditions in a 10 mM phosphate buffer at pH 7.2 for 1:10 complex/CT DNA mixtures [DNA concentration = M(nucleotide)] and are indicative of strong DNA intercalation for the cations of the dppz complexes **5** and **8**. Their ΔT_m values of +12 °C are even higher than those of +7 and +8 °C recorded for $[(\eta^5\text{-}C_5Me_5)Rh(HcysOMe)(dppz)]^{2+}$ (HcysOMe = cysteine methyl ester) and $[(\eta^5\text{-}C_5Me_5)Rh(H_2metOMe)(dppz)]^{3+}$ (H_2metOMe = L-methionine methyl ester), which exhibit strong side-on intercalation with binding constants of, respectively, 2.8×10^5 and 1.3×10^6 M^{-1} [27]. Relatively high ΔT_m values in the positive range 6–8 °C are observed for the dpq complexes **4** and **7** and the dppn complexes **6** and **9** and are indicative of possible intercalation or surface stacking of the polypyridyl ligands. Although the higher formal charge ($n = 2$) of the kinetically inert $(Me_2N)_2CS$-containing dications of **7**–**9** would be expected to lead to additional stabilization of the DNA helix through stronger electrostatic cation–phosphate interactions, no significant increases are apparent for the ΔT_m values of these complexes, in comparison to the cations of **4**–**6** with the same pp ligand. This finding suggests that rapid aquation [20] of the original monocations of **4**–**6** will afford dications of the type $[(\eta^5\text{-}C_5Me_5)Rh(H_2O)(pp)]^{2+}$ as equilibrium species for DNA interaction. In striking contrast to the $(\eta^5\text{-}C_5Me_5)Rh^{III}$ complex **4**, the ΔT_m value of only +2 °C for the analogous $(\eta^5\text{-}C_5Me_5)Ir^{III}$ species is clearly in accordance with coordinative Ir–N (nucleobase) binding.

Melting temperatures and UV/Vis-titrations for CT-DNA with the $(\eta^5\text{-}C_5Me_5)Ir^{III}$ cations $[(\eta^5\text{-}C_5Me_5)Ir(HcysOMe)(phen)]^{2+}$ and $[(\eta^5\text{-}C_5Me_5)Ir(H_2metOMe)(phen)]^{3+}$ [27] have demonstrated that the phenanthroline ligand is too small to support intercalation for this class of half-sandwich complexes. The positive ΔT_m values of 1–2 °C for these kinetically inert cations are, however, significantly higher than those in the range −5 to −1 °C observed for **1**–**3**, which can potentially bind to the nucleobase N atoms of the biopolymer. A similar ΔT_m value of −2 °C has been reported for $[(\eta^6\text{-}C_6H_6)RuCl(en)]^+$, which preferentially coordinates DNA guanine bases at their endocyclic N7 atoms [11]. ^{1}H NMR studies demonstrated that N7 coordination is complete within 5 min for 1:2 reaction mixtures of **1**–**6** with guanosine 5′-monophosphate at 30 °C. It can, therefore, be assumed that compounds **1**–**3** will rapidly bind to CT DNA through coordinative Rh–N (nucleobase) bonds. The low ΔT_m values of, respectively, +2 and +1 °C for the monocations of the kinetically inert dppz complexes **10** and **11** indicate that their aromatic thiolate ligands must impair stable DNA intercalation.

Following incubation periods of 5–30 min, UV/Vis spectra of buffered solutions of complexes **1**–**11** (10 mM phosphate buffer, pH 7.2) with CT DNA at 25 °C and $r = 0.1$ exhibit no further significant changes, thereby indicating that achievement of equilibrium conditions must be relatively rapid. Pronounced decreases in absorbance for complexes **5** and **8** at about 364 and 384 nm and shifts of these absorption maxima to higher wavelengths are indicative of dppz intercalation into the DNA double helix. The hypochromic shift $\Delta A/A$ of −47% at 364 nm with its associated red shift of 5 nm is depicted for complex **5** in Fig. 2. Similar hypo- and bathochromic shifts of respectively $\Delta A/A$ of −41% and $\Delta\lambda = 3$ nm were also observed for the analogous π–π^* transition of complex **8**. The spectral changes observed for the interaction of **5** and **8** with CT DNA are also similar to those reported for the analogous $(\eta^6\text{-}C_6Me_6)Ru^{II}$ complexes $[(\eta^6\text{-}C_6Me_6)RuCl(dppz)]^+$ and $[(\eta^6\text{-}C_6Me_6)Ru\{(Me_2N)_2CS)_2\}(dppz)]^{2+}$ [15] and the kinetically inert $(\eta^5\text{-}C_5Me_5)Ir^{III}$ complex $[(\eta^5\text{-}C_5Me_5)Ir\{(Me_2N)_2CS)_2\}(dppz)]^{2+}$ [19]. In striking contrast, $[(\eta^5\text{-}C_5Me_5)IrCl(dppz)]^+$ also exhibits initial large negative hypochromic shifts $\Delta A/A$ at 364 and 383 nm after 1 min of mixing with CT DNA, but these are followed by a steady increase in absorbance at both wavelengths. A state of equilibrium is achieved after 10 min, in which the final spectrum exhibits small absorbance increases for the π–π^* transitions in accordance with Ir–N (nucleobase) binding and negligible intercalation or surface stacking.

Kinetic studies have established that the rate constants for substitution of $(\eta^5\text{-}C_5Me_5)Rh^{III}$ complexes are much higher than for analogous $(\eta^5\text{-}C_5Me_5)Ir^{III}$ or $(\eta^6\text{-arene})Ru^{II}$ species [20]. Values of, respectively, 1.59×10^3 s^{-1}, 2.19×10^2 s^{-1} and 10.2×10^{-2} s^{-1} were determined, for instance, for the rate of water exchange at 298 K in $[(\eta^5\text{-}C_5Me_5)Rh(bpy)(H_2O)]^{2+}$, and its $[(\eta^5\text{-}C_5Me_5)Ir^{III}$ and $[(\eta^6\text{-}C_6Me_6)Ru^{II}$ analogues. As a change in the DNA interaction mode from initial intercalation to coordinative M–N (nucleobase) binding should clearly be kinetically favoured for $M = Rh^{III}$ in comparison to $M = Ir^{III}$, the retention of the former mode for the $[(\eta^5\text{-}C_5Me_5)Rh^{III}$ complexes **5** and **8** must result from its relative thermodynamic stability for the 4d transition metal. M–N (nucleobase) bonds will be significantly weaker for rhodium(III) than for its much softer 5d homologue.

Table 2
Melting temperature shifts ΔT_m, for the interaction of complexes $[(\eta^5\text{-}C_5Me_5)Rh(L)(pp)](CF_3SO_3)_n$ (**1**–**11**) with CT DNA at $r = 0.1$ in a 10 mM phosphate buffer at pH 7.2 after incubation for 60 min

Compound	pp	L	n	ΔT_m (°C)
1	en	Cl	1	−4
2	bpy	Cl	1	−5
3	phen	Cl	1	−1
4	dpq	Cl	1	+6
5	dppz	Cl	1	+12
6	dppn	Cl	1	+7
7	dpq	$(Me_2N)_2CS$	2	+8
8	dppz	$(Me_2N)_2CS$	2	+12
9	dppn	$(Me_2N)_2CS$	2	+6
10	dppz	C_6H_5S	1	+2
11	dppz	$C_{10}H_7S$	1	+1

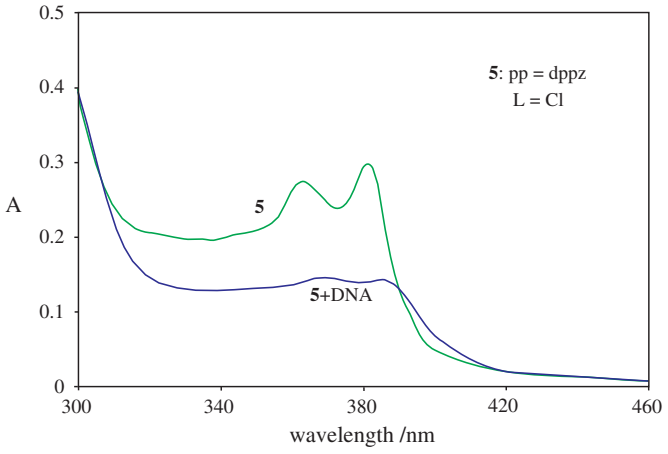

Fig. 2. UV/Vis spectra of dppz complex **5** (20 μM) and its equilibrium reaction mixture with CT DNA (200 μM) in a 10 mM phosphate buffer (pH 7.2) after 5 min.

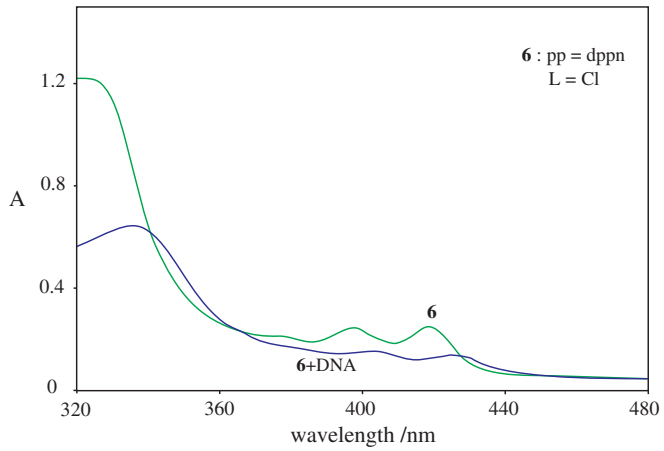

Fig. 3. UV/Vis spectra of dppn complex **6** (20 μM) and its equilibrium mixture with CT DNA (200 μM) in a 10 mM phosphate buffer (pH 7.2) after 20 min.

In similarity to the dppz complexes, significant decreases in absorbance are also observed for the dppn complexes **6** (Fig. 3) and **9** at their characteristic maxima at about 323, 398 and 420 nm. Equilibrium is achieved within 12 min for **6** and 30 min for **9** and, in contrast to the analogous $[(\eta^5\text{-}C_5Me_5)Ir^{III}$ [19] and $[(\eta^6\text{-}C_6Me_6)Ru^{II}$ complexes [15], no positive changes in the $\Delta A/A$ values are observed during this time period. The respective final $\Delta A/A$ values for **6** and **9** at the first maximum are −46% and −38%. No effective changes in absorption in the range 320–450 nm were recorded for complexes **1**–**3** (pp = en, bpy, phen) on mixing with CT DNA and the changes for complex **4** (pp = dpq) were of a minor nature. It is interesting to compare the UV/Vis spectra of 1:10 mixtures of **10** and **11** with CT DNA with those recorded for **5** and **8**. An intramolecular π–π interaction between the dppz and naphthalene aromatic systems is apparent for **11** in the solid state (Fig. 4b), as evidenced by their interplanar angle of only 11.3(3)°. As observed for the dppz complex **5**, the five-membered chelating in **11** is almost flat with an interplanar angle of 1.4(4)° between N1–Rh–N10 and N1–C–C–N10 planes. The dppz and cyclopentadienyl planes are inclined at 60.7(3)°. Low respective values of −15% and −10% for $\Delta A/A$ at 364 nm for complex/DNA mixtures of **10** and **11** indicate that such interactions are strong enough to prevent a significant degree of intercalation. Fig. 4a depicts the molecular structure of the $[(\eta^5\text{-}C_5Me_5)Rh\{(Me_2N)_2CS)_2\}(dpq)]^+$ cation **7**, whose dppz and dppn analogues **8** and **9** exhibit large negative values of $\Delta A/A$ for π–π^* transitions on mixing with DNA. It is apparent that the steric bulk of tetramethyl thiourea ligand will be greater than that of the benzenethiolate ligand in **10**, whose

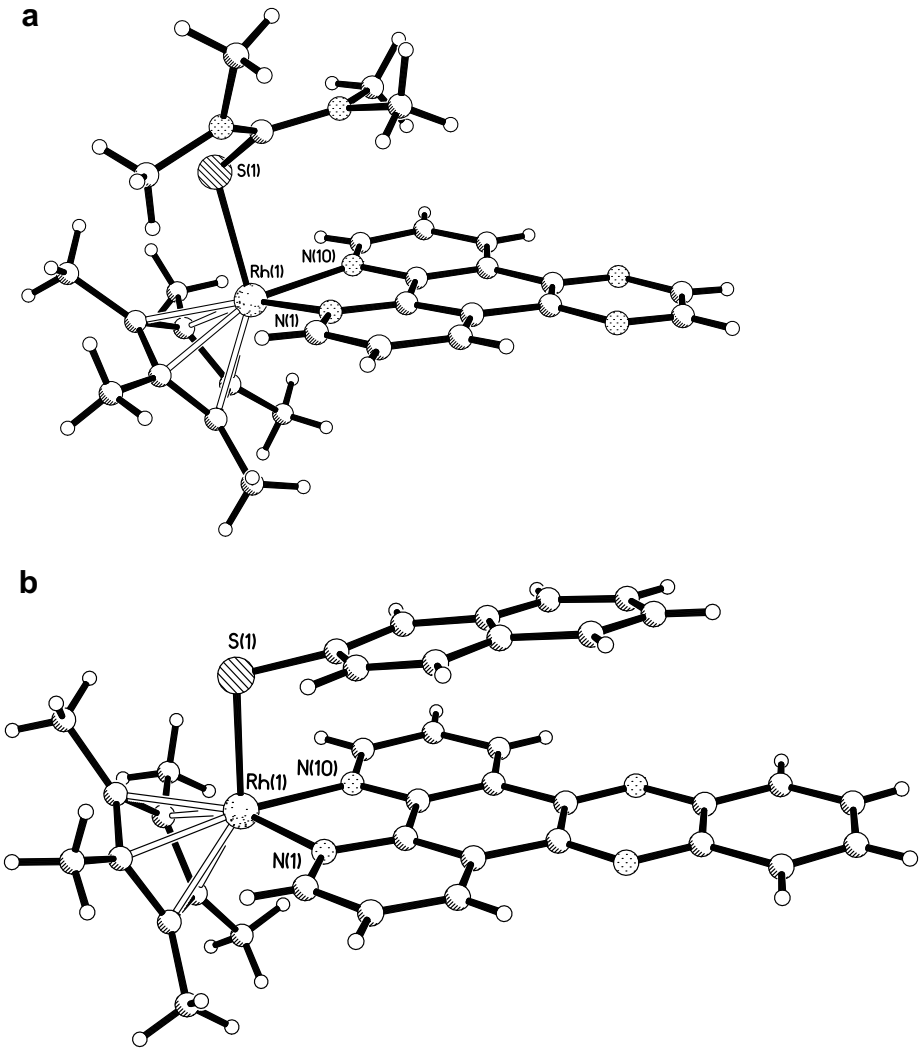

Fig. 4. Molecular structures of the cations of: (a) $[(\eta^5\text{-}C_5Me_5)Rh(dpq)\{(Me_2N)_2CS\}](CF_3SO_3)_2$ (**7**) and (b) $[(\eta^5\text{-}C_5Me_5)Rh(C_{10}H_7S)(dppz)](CF_3SO_3)$ (**11**).

volume requirements can be estimated from the molecular structure of the analogous $[(\eta^5\text{-}C_5Me_5)Rh(dppz)(C_{10}H_7S)]^+$ cation of **11** (Fig. 4b). The observation of intercalation for **8** but not for **10** indicates that the intramolecular π–π interactions may be retained for the latter complex on interaction with CT DNA. In contrast to dpq complex **4**, the N1–Rh1–N10 plane in **7** is titled below and not above the plane of the polypyridyl ligand, presumably due to steric repulsion between $(Me_2N)_2CS$ methyl groups and dpq atoms. This distortion leads to a much smaller interplanar angle of 44.3(5)° between the cyclopentadienyl and dpq planes in comparision to that of 76.6(2)° in **4**. The N1–Rh1–N10 plane is inclined at 10.5(9)° to the N1–Rh1–N10 plane of the chelate ring.

2.2.2. Circular dichroismus

Characteristic changes in the observed circular dichroismus (CD) spectra of DNA in the range 220–350 nm provide a convenient means of monitoring conformational changes for the biopolymer [30,31]. A negative CD band at 246 nm caused by the helical B conformation and a positive band at 275 nm due to base stacking are observed for CT DNA [31]. Addition of the complexes **1**–**3** (pp = en, bpy, phen) at a 1:10 complex/[DNA] molar ratio leads to only minor spectral changes, thereby indicating little distortion of the B helix on formation of Rh–N (nucleobase) bonds to the biopolymer. Although aromatic molecules often generate CD bands between 260 and 400 nm on interaction with DNA, the presence of such signals is not necessarily of relevance for the assignment of the binding mode. The observed induced circular dichroismus is caused by the rigid orientation of the molecule with respect to the double helix and this can also result from coordinative, surface or groove binding in addition to intercalation. As depicted in Fig. 5, the complexes **5** and **8** do, however, exhibit characteristic negative CD bands with molar ellipticities $[\theta]$ of -3.4×10^{-3} and -4.5×10^{-3} deg cm^2 mol^{-1} at $\lambda = 296$ nm and it has previously been established [15,19,29] that the appearance of such bands is, indeed, characteristic for dppz intercalation. The significant increases and the blue shifts of the positive CD bands at 268 nm may of be attributed to resulting changes in the base stacking of the double helix.

In contrast to **5** and **8**, the dppz complexes **10** and **11** do not exhibit negative induced CD bands at about $\lambda = 300$ nm. This finding is in accordance with an absence of significant DNA intercalation, as was indicated for these complexes by their low ΔT_m and

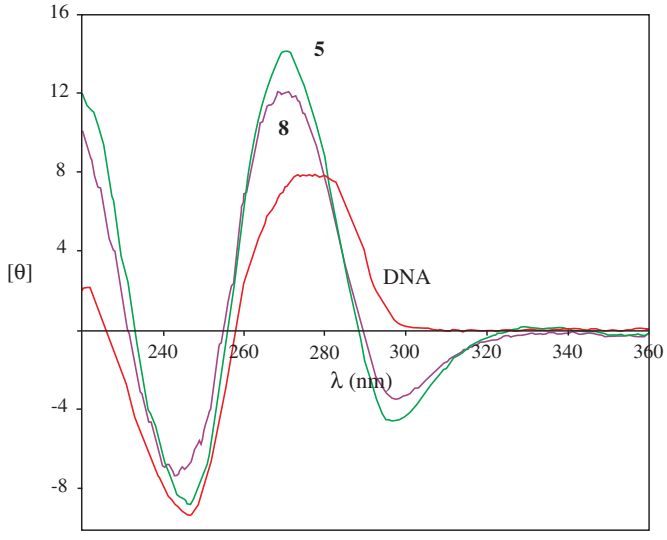

Fig. 5. CD spectra of CT DNA and mixtures of $[(\eta^5\text{-}C_5Me_5)RhCl(dppz)]$ (CF_3SO_3) (**5**) and $[(\eta^5\text{-}C_5Me_5)Rh(dppz)\{(Me_2N)_2CS\}](CF_3SO_3)_2$ (**8**) with CT DNA ($r = 0.1$) in a 10 mM phosphate buffer (pH 7.2) after 2 h incubation.

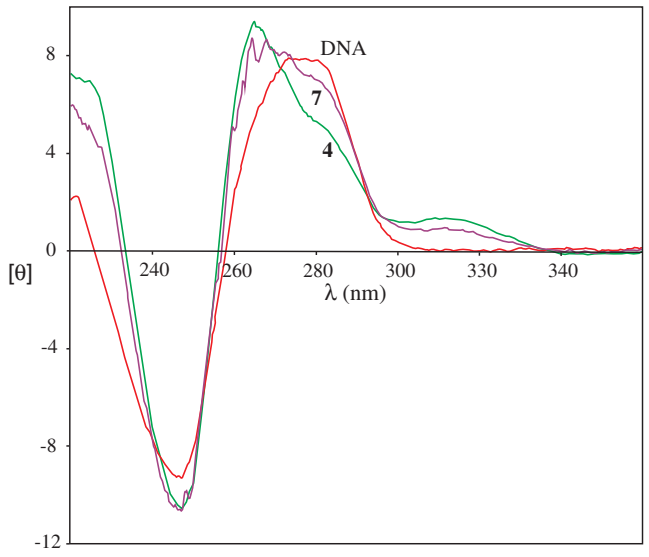

Fig. 6. CD spectra of CT DNA and mixtures of $[(\eta^5\text{-}C_5Me_5)$ $RhCl(dpq)]$ (CF_3SO_3) (**4**) and $[(\eta^5\text{-}C_5Me_5)Rh(dpq)\{(Me_2N)_2CS\}](CF_3SO_3)_2$ (**7**) with CT DNA in a 10 mM phosphate buffer (pH 7.2) after 2 h incubation.

$-\Delta A/A$ values. When compared to the CD spectrum of CT DNA alone, a broadening and apparent splitting are, however, discernable for the positive bands of the 1:10 mixture of the dpq complexes **4** and **7** with the biopolymer (Fig. 6). As **4** and **7** both exhibit absorption maxima for spin-allowed MLCT π–π^* transitions at $\lambda = 260$ and 300 nm, it is probable that the shape of the bands in the 270–295 nm range will be due to spectral overlap with a negative CD contribution caused by intercalating dpq ligands. A similar shape has been observed for the positive band of a mixture of the intercalating complex $[(\eta^6\text{-}C_6Me_6)RuCl(dpq)](CF_3SO_3)$ with CT DNA [15] and this is accompanied by an additional positive band at 315 nm, as is also the case for complexes **4** and **7**. The CT DNA bands in the range 220–300 nm exhibit only minor changes following incubation with the dppn complexes **6** and **9** for 2 h and remain unchanged over a period of 24 h. Similar observations were also made for the analogous chlorido cations $[(\eta^5\text{-}C_5Me_5)IrCl(dppn)]^+$ and $[(\eta^6\text{-}C_6Me_6)RuCl(dppn)]^{2+}$ [19,15]. In contrast, the interaction with $[(\eta^5\text{-}C_5Me_5)Ir\{(R_2N)_2CS\}(dppn)]^{2+}$ (R = H, Me) and $[(\eta^6\text{-}C_6Me_6)Ru\{(H_2N)_2CS\}(dppn)]^{2+}$ leads to massive changes in the original B DNA conformation. The negative band at about 246 nm disappears in all three cases and the resulting CD spectrum for the $(\eta^6\text{-}C_6Me_6)Ru^{II}$ complex is in accordance with DNA damage and complete loss of the B-helix conformation. A large increase in $[\Theta]$ to 10.2×10^3 deg cm^2 mol^{-1} for the positive CD bands of the $[(\eta^5\text{-}C_5Me_5)Ir\{(Me_2N)_2CS\}(dppn)]^{2+}$/CT DNA mixture is indicative of the possible adoption of an A DNA conformation.

2.2.3. Viscosity measurements

The most convincing evidence for DNA intercalation is provided by viscosity measurements [32,33]. Insertion of aromatics ligands such as dpq or dppz between adjacent nucleobase pairs leads to lengthening and stiffening of the double helix and these changes are reflected in an increase in DNA viscosity. Fig. 7 illustrates the dependence of the logarithmic relative reduced viscosity $\ln(\eta/\eta_0)$ on the concentration function $\ln(1 + r)$ (r = [complex]/[DNA]] for the chlorido complexes **4**–**6**. Effective intercalation is confirmed by the slope values of 2.74 and 2.17 for the complexes **4** (pp = dpq) and **5** (pp = dppz), in accordance with CD observations. Large increases in $\ln(\eta/\eta_0)$ are also found for the likewise intercalating $(Me_2N)_2CS$ complexes **7** (pp = dpq) and **8** (pp = dppz) with their

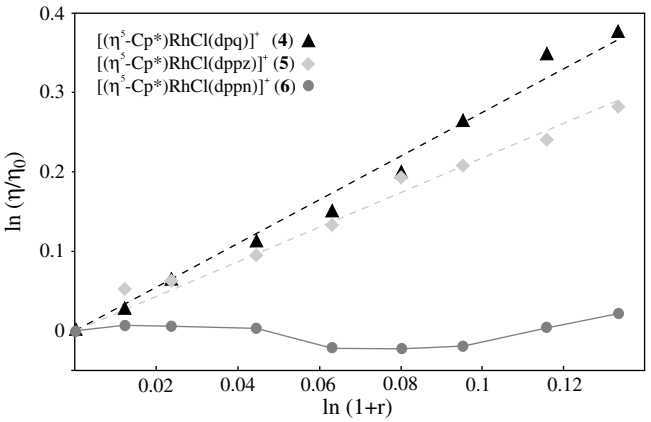

Fig. 7. Viscometric titrations of sonicated DNA with the chlorido complexes **4**–**6** (pp = dpq, dppz, dppn) in a 10 mM phosphate buffer at pH 7.2; η = reduced vicosity of the DNA solution in the presence of a complex, η_0 = reduced vicosity of the DNA solution alone, r = [complex]/[DNA].

respective slope values being 2.66 and 1.44. In contrast to the dpq and dppz complexes, significant DNA lengthening is not observed for the dppn complexes **6** and **9** in the 0.0–0.08 range for $\ln(1 + r)$. It can, therefore, be concluded that coordinative Rh–N (nucleobase) binding will probably be predominant for the chlorido complex **6** and electrostatic surface interactions for $(Me_2N)_2CS$ complex **9** at low values of r. Interestingly, a small but steady increase is observed for the relative reduced velocity $\ln(\eta/\eta_0)$ of both complexes at $\ln(1 + r)$ values greater than 0.08. This suggests that surface stacking of adjacent dppn ligands could cause DNA lengthening at higher [complex]/[DNA] ratios. The presence of such interactions is clearly indicated by the significant decreases in absorbance for the π–π^* transitions of complexes **6** (Fig. 3) and **9** at $r = 0.1$.

The failure of the large dppn ligand to exhibit significant DNA intercalation in its $(\eta^5\text{-}C_5Me_5)Rh^{III}$ and $(\eta^6\text{-}C_6Me_6)Ru^{II}$ [15] complexes is in striking contrast to findings for other types of transition metal complexes. For instance, a binding constant $K_b = 7.8 \times 10^4\ M^{-1}$ and site size s of 1.4 have been recently determined for the complex $[Ir(dppn)(ppy)_2](PF_6)$ (Hppy = 2-phenylpyridine) [34]. This K_b value is significantly larger than that of $2.0 \times 10^4\ M^{-1}$ (site size $s = 1.3$) obtained for the analogous dppz complex, in agreement with similar measurements for rhenium(I) complexes [35,36] and $(tpm)Ru^{II}$ complexes of the type $[(tpm)\text{-}RuCl(pp)]^+$ (tpm = tris(1-pyrazolyl)methane; pp = dppn, dppz) [37]. These findings are in accordance with the results of Sartorius and Schneider [38] for heterocyclic derivatives with positively charged ammonium groups in their side chains. These authors found that the intercalation binding strength is essentially a function of the size of the aromatic system, independent of the heteroatoms or the presence of local positive charges within the planar moieties. The apparent lack of stable intercalation for complexes **6** and **9** and for analogous $(\eta^6\text{-}C_6Me_6)Ru^{II}$ complexes must, therefore, be attributed to their preferred side-on intercalation mode [27,28]. Close non-bonding contacts to the DNA backbone would be inevitable for the atoms of the additional six-membered ring of dppn and may prevent its suitable side-on alignment between the nucleobases of B DNA. Massive conformational distortions and a possible B to A DNA change are necessary to facilitate dppn intercalation for $[(\eta^5\text{-}C_5Me_5)Ir\{(Me_2N)_2CS\}(dppn)]^{2+}$ [19]. Small decreases in the reduced viscosity were recorded for mixtures of the complexes **1**–**3** with CT DNA at r values in the range 0.08–0.12. These decreases may be due to kinking or bending of the double helix [39,40] caused by hydrophobic interactions with the DNA surface or by intermolecular interactions between coordinating metal fragments.

2.3. Cellular uptake

We have previously demonstrated that the cytotoxicity of complexes of the types $[(\eta^6\text{-}C_6Me_6)RuCl(pp)]^+$ and $[(\eta^6\text{-}C_6Me_6)Ru\{(NH_2)_2CS\}(pp)]^{2+}$ is governed by the size of the polypyridyl ligand (pp = dpq, dppz, dppn) and the resulting cellular uptake efficiency [15]. Owing to their decreased lipophilicity, cellular ruthenium levels are much lower for the latter dicationic thiourea complexes than for the monocationic chlorido species and this causes a decrease in cytotoxicity. In order to evaluate the influence of cellular uptake on the cytotoxicity of $(\eta^5\text{-}C_5Me_5)Rh^{III}$ complexes, we quantified the rhodium concentrations in tumour cells exposed to **1**–**11** by atomic absorption spectroscopy. The similar ΔT_m values (Section 2.2.1) for pairs of $(\eta^5\text{-}C_5Me_5)Rh^{III}$ complexes **4**/**7**, **5**/**8** and **6**/**9** with the same polypyridyl ligand indicate that **4**–**6** must be present as dications $[(\eta^5\text{-}C_5Me_5)Rh(H_2O)(pp)]^{2+}$ following rapid aquation. As a result of this increase in cation charge, levels of cellular uptake (Table 3) are low for complexes **4**–**6** (and **1**–**3**) and comparable with the values established for the kinetically inert dicationic complexes **7**–**9**. The small increases in intracellular rhodium levels for the latter complexes (compare the pairs **4**/**7**, **5**/**8** and **6**/**9**) may be due to the presence of hydrophobic $(Me_2N)_2CS$ ligands rather than coordinating water molecules. This result is of special interest as the opposite trend was expected based on the fact that **7**–**9** represent dicationic species, which are supposedly less lipophilic than the monocationic complexes **4**–**6**. A trend to increased uptake efficiency is apparent for both series, in accordance with increasing lipophilicity of the polypyridyl ligands in the order of increasing size dpq < dppz < dppn. However, 100 μM concentrations of these complexes are necessary to achieve cellular levels similar to those obtained for 10 μM solutions of analogous $(\eta^5\text{-}C_5Me_5)Ir^{III}$ and $(\eta^6\text{-}C_6Me_6)Ru^{II}$ dications. For instance, similar cellular metal levels of respectively 150 ng Ir/mg protein (=0.78 nmol Ir/mg protein) and 85 ng Ru/mg protein (=0.84 nmol Ru/mg protein) were determined

Table 3
Cellular rhodium levels [ng(Rh)/mg(protein)] in MCF-7 and HT-29 tumour cells after exposure to given concentrations of complexes $[(\eta^5\text{-}C_5Me_5)Rh(L)(pp)](CF_3SO_3)_n$ (**1**–**11**) for 4 h

Compound	pp	L	n	c (μM)	MCF-7	HT-29
*(i) Complexes **1**–**11***						
1	en	Cl	1	100	4.9(2.7)	4.4(3.2)
2	bpy	Cl	1	100	14.2(9.1)	10.7(3.1)
3	phen	Cl	1	100	11.9(2.9)	10.1(1.9)
4	dpq	Cl	1	100	11.3(0.5)	4.1(1.7)
5	dppz	Cl	1	100	45.0(2.5)	42.2(4.4)
6	dppn	Cl	1	10	1.8(∗)	3.5(1.2)
				100	189.3(15.5)	378.1(66.0)
7	dpq	$(Me_2N)_2CS$	2	100	18.7(1.7)	15.2(2.8)
8	dppz	$(Me_2N)_2CS$	2	100	90.5(6.1)	77.7(3.7)
9	dppn	$(Me_2N)_2CS$	2	10	5.1(∗)	6.7(0.9)
				100	217.1(12.0)	331.5(25.2)
10	dppz	C_6H_5S	1	1	59.2(2.8)	20.7(9)
				10	453.3(37.9)	84.8(20.3)
				100	2337(122.8)	1137.1(174.7)
11	dppz	$C_{10}H_7S$	1	1	76.1(29.2)	17.8(2.2)
				10	398.9(44.2)	303.7(47.9)
				100	2904(132.3)	2029(36.5)
(ii) Analogous iridium(III) complexes [15,19]						
5(Ir)	dppz	Cl	1	10	n.d.	70.4(1.0)
				100	n.d.	556.1(32.3)
9(Ir)	dppn	$(Me_2N)_2CS$	2	10	n.d.	149.6(7.8)
				100	n.d.	906.3(117.6)

The values in brackets represent the standard errors (∗, single value; n.d., not determined).

for HT-29 cells following incubation periods of 4 h with 10 μM solutions of $[(\eta^5\text{-}C_5Me_5)Ir\{(NMe_2)_2CS\}(dppn)]^{2+}$ [41] and $[(\eta^6\text{-}C_6Me_6)Ru\{(NH_2)_2CS\}(dppn)]^{2+}$ [15]. For the corresponding complexes **6** and **9** at 10 μM concentrations significantly lower values were found (below 10 ng (=0.10 nmol) Rh/mg protein in all experiments). The low value of 70.4 ng Ir/mg protein observed for $[(\eta^5\text{-}C_5Me_5)IrCl(dppn)]^+$ suggests that this complex must also be present as an aqua dication following rapid H_2O/Cl^- exchange. In striking contrast, a cell uptake of 1054.7 ng Ru/mg protein was measured for a 10 μM solution of the analogous $(\eta^6\text{-}C_6Me_6)Ru^{II}$ complex, for which the aquation rate is much lower.

The influence of cation charge on the level of cellular uptake is clearly apparent for the monocations of $[(\eta^5\text{-}C_5Me_5)Rh(L)(dppz)](CF_3SO_3)$ **10** (L = $C_6H_5S^-$) and **11** (L = $C_7H_{10}S^-$), where intracellular levels for 1 μM solutions are comparable with those established for 100 μM solutions of the dppz dications of **5** and **8**. Increased lipophilicity due to the presence of aromatic thiolate ligands may also play a role in improving complex passage through the cell membrane for **10** and **11**.

2.4. Cytotoxicity measurements

IC_{50} values for the complexes **1**–**11** towards MCF-7 and HT-29 cells are listed in Table 4. As previously reported for analogous $(\eta^6\text{-}C_6Me_6)Ru^{II}$ complexes [15], the cytotoxicity of members of the series **4**–**6** and **7**–**9** is directly correlated to the surface area of the polypyridyl ligand (pp = dpq, dppz, dppn) and, therefore, to the level of cellular uptake. However the increases in cytotoxicity within the series dpq < dppz < dppn are much less pronounced than for the monocations $[(\eta^6\text{-}C_6Me_6)RuCl(pp)]^+$, where, for instance, the IC_{50} value for HT-29 cells decreases from 30.3 over 2.5 to 0.4 μM [15]. This weakening of the polypyridyl ligand influence for $(\eta^5\text{-}C_5Me_5)Rh^{III}$ complexes is most apparent for pp = dppn and is clearly a result of the very low levels of cellular uptake for the aqua dications of **4**–**6** and the $(Me_2N)_2CS$ dications of **7**–**9**. It should be noted that we also observed cytotoxic effects for the free polypyridyl ligands, which increase in the order bpy < phen, dpq < dppz < dppn (Table 4). The similarity of the IC_{50} values for the pp ligands and their $(\eta^5\text{-}C_5Me_5)Rh^{III}$ complexes provides strong evidence for the dominant influence of the polypyridyl surface area on the cytotoxic activity of **2**–**11**.

In this context, it is interesting to observe that the IC_{50} values for half-sandwich dppz complexes all lie within fairly narrow ranges (MCF-7, 1.5–2.5 μM; HT-29, 2.5–7.4 μM) independent of the organometallic fragment, the overall cation charge and the nature of the non-polypyridyl ligands. Values of 2.1/2.5 and 2.5/6.7 μM were reported for MCF-7/HT-29 following incubation with $[(\eta^6\text{-}C_6Me_6)RuCl(dppz)]^+$ and $[(\eta^6\text{-}C_6Me_6)Ru\{(NH_2)_2CS\}(dppz)]^{2+}$, respectively [15]. In contrast to the dppz complexes, significant differences are, however, apparent for both the smaller and larger polypyridyl ligands. Despite their much poorer cell uptake, the dications of the dpq complexes **4** and **7** are some 2–3 times more active than $[(\eta^6\text{-}C_6Me_6)RuCl(dpq)]^+$, for which IC_{50} values of 11.1 and 30.5 μM were established for MCF-7 and HT-29, respectively. The improvement in cytotoxicity is even more striking for the phen complex **3**, which exhibits promising IC_{50} values of 4.7 and 8.0 μM against MCF-7 and HT-29 cells. In contrast, previously tested complexes of the type $[(\eta^6\text{-indan})RuCl(pp)]^+$ containing phenanthroline derivatives all show poor or no activity towards human A2780 cells (ovarian cancer) [2] and $[(\eta^5\text{-}C_5Me_5)IrCl(phen)]^+$ is inactive for MCF-7 and HT-29 cells. As both the en and bpy complexes **1** and **2** do not exhibit no significant cytotoxicity against these cell lines (Table 4), it can be assumed that cellular interactions involving the phen aromatic system must be responsible for the activity of complex **3**.

These observations for phen and dpq complexes indicate that the nature of the organometallic fragment can significantly influence the cytotoxicity of complexes containing smaller polypyridyl ligands. The DNA binding studies and the results of the cellular uptake and cytotoxicity investigations suggest that initial DNA recognition [42] and intercalation rather than kinetically controlled coordinative Rh–N(DNA) binding may be of central importance in determining the biological activity of the polypyridyl complexes **4**–**11**. A case in point is provided by the thiolate complexes **10** and **11**, whose monocations exhibit much better cellular uptake values than those established for the dications of **5** and **8**. **10** and **11** are indeed, respectively, 2.3 and 2.7 more active towards MCF-7 cells but significant improvements are not observed for HT-29 cells. It seems probable that the impairment of intercalation caused by intramolecular stacking of the dppz ligands with the thiolate aromatic systems, will restrict possible increases in cytotoxicity due to the much higher intracellular concentrations of the complexes. An instructive example for the importance of DNA interactions is given by dppn complex **9** and its $(\eta^5\text{-}C_5Me_5)Ir^{III}$ counterpart (Tables 3 and 4), whose IC_{50} values for MCF-7 and HT-29 cells are, respectively, some 5.4 and 8.8 times lower than for the $(\eta^5\text{-}C_5Me_5)Rh^{III}$ complex. A possible explanation is provided by the fact that the $(\eta^5\text{-}C_5Me_5)Ir^{III}$ complex exhibits strong intercalative binding, which leads to a possible B to A change in the DNA conformation [19], whereas only surface stacking is observed for the dppn ligand of the $(\eta^5\text{-}C_5Me_5)Rh^{III}$ analogue. This example also demonstrates that the nature of the metal fragment can in certain cases significantly influence the cytotoxicity of its polypyridyl complexes, even when one of the larger pp ligands (dppz, dppn) is present.

Table 4
IC_{50} values (μM)[a] for the complexes $[(\eta^5\text{-}C_5Me_5)Rh(L)(pp)](CF_3SO_3)_n$ (**1**–**11**)

Compound	pp	L	*n*	MCF-7	HT-29
*(i) Complexes **1**–**11***					
1	en	Cl	1	>100	>100
2	bpy	Cl	1	>100	>100
3	phen	Cl	1	4.7(0.1)	8.0(1.6)
4	dpq	Cl	1	5.1(0.2)	8.5(0.3)
5	dppz	Cl	1	1.5(0.4)	4.3(0.2)
6	dppn	Cl	1	0.8(0.1)	3.2(0.5)
7	dpq	$(Me_2N)_2CS$	2	5.3(0.7)	10.7(0.5)
8	dppz	$(Me_2N)_2CS$	2	1.5(0.1)	4.3(0.1)
9	dppn	$(Me_2N)_2CS$	2	0.91(0.06)	3.6(0.5)
10	dppz	C_6H_5S	1	0.64(0.08)	6.1(0.5)
11	dppz	$C_{10}H_7S$	1	0.56(0.25)	3.3(0.2)
(ii) Polypyridyl ligands					
	bpy			52.7(7.8)	45.7(4.6)
	phen			3.5(0.2)	2.7(0.5)
	dpq			6.7(2.0)	7.0(2.2)
	dppz			0.8(0.6)	1.8(0.2)
	dppn			0.15(0.05)	n.d.
(iii) Analogous iridium(III) complexes [15,19]					
5(Ir)	dppz	Cl	1	2.3(0.4)	7.4(0.9)
9(Ir)	dppn	$(Me_2N)_2CS$	2	0.17(0.02)	0.41(0.16)
(iv) Cisplatin			2.0(0.3)	7.0(2.0)	

[a] Towards the human cancer cell lines MCF-7 (breast cancer) and HT-29 (colon cancer); the values in brackets represent the standard errors.

3. Conclusions

We have demonstrated that the DNA binding of polypyridyl organorhodium(III) complexes of the types $[(\eta^5\text{-}C_5Me_5)RhCl(pp)](CF_3SO_3)$ **1**–**6** and $[(\eta^5\text{-}C_5Me_5)Rh\{(Me_2N)_2CS\}(pp)](CF_3SO_3)_2$ **7**–**9** is governed by the size of the polypyridyl ligand. Whereas stable intercalative binding is observed for the dpq complexes **4** and **7** and the dppz complexes **5** and **8**, the surface area of the dppn

ligand of **6** and **9** is apparently too large to support stable side-on intercalation. Intramolecular interactions between the aromatic systems of the thiolate L^- and dppz ligands appear to prevent significant DNA intercalation for [(η^5-C_5Me_5)Rh(L)-(pp)](CF_3SO_3), **10** (L = $C_6H_5S^-$) and **11** (L = $C_{10}H_7S^-$).

Rapid Cl^-/H_2O exchange leads to formation of aqua dications for complexes **1**–**6** and similar low levels of cellular uptake are observed for **4**–**6** and their kinetically inert $(Me_2N)_2CS$ analogues **7**–**9**. The cytotoxicity of the latter compounds **4**–**9** is governed by the size of the polypyridyl ligands with IC_{50} values varying in the order dppn < dppz < dpq. An exception to this rule is provided by the phen complex **3**, whose IC_{50} values of 4.7 and 8.0 μM against MCF-7 and HT-29 cells are comparable with those observed for the dpq complexes **4** and **7**.

4. Experimental

Solvents were dried and distilled before use. ^1H and ^{13}C NMR spectra were recorded on a Bruker DRX 400 spectrometer and LSIMS data (liquid secondary ion mass spectrometry) on a VG Autospec instrument using 3-nitrobenzyl alcohol as the matrix. ^{13}C NMR signals for the $CF_3SO_3^-$ anions of **1**–**11** were observed in the δ range 121.8–122.8 ppm and are not listed for individual complexes. An analytik jena SPECORD 200 was employed for UV–Vis measurements and CD spectra were registered on a Jasco J-715 instrument in the range 220–400 nm for 1:10 complex/[DNA] mixtures [DNA concentrations in M(nucleotide)] in a 10 mM phosphate buffer at pH 7.2. Elemental analysis were performed on a Vario El (Elementar Analysensysteme). $RhCl_3 \cdot 3H_2O$ and $Ag(CF_3SO_3)$ were obtained from Chempur, 2,2′-bipyridine (bpy), 1,10-phenanthroline (phen), and tetramethyl thiourea from Acros, ethylenediamine (en) from Riedel de Haen and 1-benzenethiol and 2-naphthalenethiol from TCI. Solvents were purchased from TJ Baker and DEUTERO GmbH and NaOMe from Merck. The starting complex [{(η^5-C_5Me_5)RhCl}$_2$(μ-Cl)$_2$] [43] and the polypyridyl ligands dpq [44], dppz [45] and dppn [34] and [(η^5-C_5Me_5)RhCl(dppz)](CF_3SO_3) (**5**) [27] were synthesised according to literature procedures.

4.1. Preparation of 1–4 and 6–11

4.1.1. [(η^5-C_5Me_5)RhCl(en)](CF_3SO_3) (1)

Two equivalents of $Ag(CF_3SO_3)$ (51.4 mg, 0.2 mmol) were added to [{(η^5-C_5Me_5)RhCl}$_2$(μ-Cl)$_2$] (61.8 mg, 0.1 mmol) in 10 ml acetone and stirred in the dark for 0.5 h. Filtration of the resulting AgCl precipitate and subsequent solvent removal under vacuum afforded [(η^5-C_5Me_5)RhCl(acetone)$_2$](CF_3SO_3), which was stirred with the ligand ethylenediamine (en) (13.5 μl, 0.2 mmol) in CH_3OH/CH_2Cl_2 (1:1, 10 ml) at 75 °C for 2 h. Following cooling and solvent removal under vacuum, the resulting solid was dissolved in 3 ml CH_3OH. The product was subsequently precipitated by addition of diethyl ether, washed and dried in vacuo. Yield: 71% (68 mg). $C_{13}H_{23}ClF_3N_2O_3RhS$; M = 482.7 g/mol. Anal. Calc.: C, 32.3; H, 4.8; N, 5.8; S, 6.7. Found: C, 32.0; H, 4.8; N, 5.9; S, 6.7%. LSIMS: m/z 447 (65%) $[M-Cl]^+$, 333 (100%) $[M-CF_3SO_3]^+$, 297 (35%) $[M-CF_3SO_3-Cl]^+$. ^1H NMR (d_6-DMSO, 30 °C): δ = 1.68 (s, 15H, Cp^*-CH_3), 2.33 (mm, 2H, en-CH_2), 2.53 (m, 2H, en-CH_2), 4.31 (m, 2H, en-NH_2), 5.02 (m, 2H, en-NH_2) ppm. ^{13}C NMR (d_6-DMSO, 30 °C): δ = 8.4 (Cp^*-C**C**H_3), 44.2 (en-**C**H_2), 93.6 (Cp^*-**C**CH_3) ppm.

4.1.2. [(η^5-C_5Me_5)RhCl(2,2′-bpy)](CF_3SO_3) (2)

Preparation as for 1 with the ligand bpy (31.3 mg, 0.2 mmol). Yield: 76% (87 mg). $C_{21}H_{23}ClF_3N_2O_3RhS$; M = 578.8 g/mol; Anal. Calc.: C, 43.6; H, 4.0; N, 4.8; S, 5.5. Found: C, 43.5; H, 4.0; N, 4.8; S, 5.4%. LSIMS: m/z 580 (6%) $[M]^+$, 543 (36%) $[M-Cl]^+$, 429 (100%) $[M-CF_3SO_3]^+$, 393 (45%) $[M-CF_3SO_3-Cl]^+$. ^1H NMR (d_6-DMSO, 30 °C): δ = 1.67 (s, 15H, Cp^*-CH_3), 7.87 (dd, 2H, H4/H4′), 8.33 (dd, 2H, H5/H5′), 8.68 (d, 2H, H6/H6′), 8.97 (d, 2H, H3/H3′) ppm. ^{13}C NMR (d_6-DMSO, 30°C): δ = 8.4 (Cp^*-C**C**H_3), 96.8 (Cp^*-**C**CH_3), 123.7, 128.3, 140.3, 152.2 (bpy-**C**H), 153.9 (bpy-**C**) ppm.

4.1.3. [(η^5-C_5Me_5)RhCl(1,10-phen)](CF_3SO_3) (3)

Preparation as for **1** with the ligand phen (36 mg, 0.2 mmol). Yield: 85% (103 mg). $C_{23}H_{23}ClF_3N_2O_3RhS$; M = 602.9 g/mol. Anal. Calc.: C, 45.8; H, 3.8; N, 4.6; S, 5.3. Found: C, 45.3; H, 3.8; N, 4.6; S, 5.6%. LSIMS: m/z 604 (10%) $[M]^+$, 567 (70%) $[M-Cl]^+$. 453 (100%) $[M-CF_3SO_3]^+$, 417 (42%) $[M-CF_3SO_3-Cl]^+$. ^1H NMR (d_6-DMSO, 30 °C): δ = 1.74 (s, 15H, Cp^*-CH_3), 8.20 (dd, 2H, H3/H8), 8.33 (s, 2H, H5/H6), 8.95 (d, 2H, H4/H7), 9.39 (d, 2H, H2/H9) ppm. ^{13}C NMR (d_6-DMSO, 30 °C): δ = 8.5 (Cp^*-C**C**H_3), 96.9 (Cp^*-**C**CH_3), 127.0, 127.6, 139.0, 152.4 (phen-**C**H), 130.0, 144.7(phen-**C**) ppm.

4.1.4. [(η^5-C_5Me_5)RhCl(dpq)](CF_3SO_3) (4)

Preparation as for **1** with the ligand dpq (46.5 mg, 0.2 mmol). Yield: 83% (108 mg). $C_{25}H_{23}ClF_3N_4O_3RhS$; M = 654.9 g/mol; Anal. Calc.: C, 45.8; H, 3.5; N, 8.6; S, 4.9. Found: C, 45.8; H, 3.5; N, 8.6; S, 4.9%. LSIMS: m/z 505 (100%) $[M-CF_3SO_3]^+$, 469 (60%) $[M-CF_3SO_3-Cl]^+$. ^1H NMR (d_6-DMSO, 30 °C): δ = 1.77 (s, 15H, Cp^*-CH_3), 8.38 (dd, 2H, H3/H8), 9.35 (s, 2H, H11/H12), 9.51 (d, 2H, H4/H7), 9.72 (d, 2H, H2/H9) ppm. ^{13}C NMR (d_6-DMSO, 30 °C): δ = 8.5 (Cp^*-C**C**H_3), 97.0 (Cp^*-**C**CH_3), 128.1, 128.7, 135.4, 153.7 (dpq-**C**H), 138.8, 146.3, 146.8 (dpq-**C**) ppm.

4.1.5. [(η^5-C_5Me_5)RhCl(dppn)](CF_3SO_3) (6)

Preparation as for **1** with the ligand dppn (66.5 mg, 0.2 mmol). Yield: 68% (107 mg). $C_{33}H_{27}ClF_3N_4O_3RhS \cdot 2H_2O$; M = 791.0 g/mol; Anal. Calc.: C, 50.1; H, 3.9; N, 7.1; S, 4.0. Found: C, 50.0; H, 3.9; N, 7.0; S, 4.2%. LSIMS: m/z 605 (100%) $[M-CF_3SO_3]^+$, 569 (75%) $[M-CF_3SO_3-Cl]^+$. ^1H NMR (d_6-DMSO, 30 °C): δ = 1.77 (s, 15H, Cp^*-CH_3), 7.74 (dd, 2H, H13/H14), 8.42 (dd, 2H, H3/H8), 8.47 (dd, 2H, H12/H15), 9.18 (s, 2H, H11/H16), 9.44 (dd, 2H, H4/H7), 9.75 (dd, 2H, H2/H9) ppm. ^{13}C NMR (d_6-DMSO, 30 °C): δ = 8.5 (Cp^*-C**C**H_3), 97.1 (Cp^*-**C**CH_3), 127.9, 128.5, 128.6, 129.8, 129.9, 135.7 (dppn-**C**H), 134.5, 137.9, 140.4, 148.3, 153.9 (dppn-**C**) ppm.

4.1.6. [(η^5-C_5Me_5)Rh(dpq){SC(NMe_2)$_2$}](CF_3SO_3)$_2$ (7)

Two equivalents of $Ag(CF_3SO_3)$ (51.4 mg, 0.2 mmol) were added to [{(η^5-C_5Me_5)RhCl}$_2$(μ-Cl)$_2$] (61.8 mg, 0.1 mmol) in 10 ml acetone and stirred in the dark for 0.5 h. Filtration of the resulting AgCl precipitate and subsequent solvent removal under vacuum yielded [(η^5-C_5Me_5)RhCl(acetone)$_2$](CF_3SO_3), which was stirred with the ligand dpq (46.5 mg, 0.2 mmol) in CH_3OH/CH_2Cl_2 (1:1, 10ml) at 75 °C for 2 h. Following cooling and solvent removal under vacuum, the red product [(η^5-C_5Me_5)RhCl(dpq)](CF_3SO_3) (**4**) was dissolved in 10 ml acetone and stirred in the dark for 0.5 h with $Ag(CF_3SO_3)$ (51.4 mg, 0.2 mmol). After filtration of the resulting AgCl precipitate and solvent removal red [(η^5-C_5Me_5)Rh(acetone)(dpq)](CF_3SO_3)$_2$ was stirred with $(Me_2N)_2CS$ (26.5 mg, 0.2 mmol) for 2 h in CH_3OH/CH_2Cl_2 (1:1, 10 ml) at 75 °C. Following cooling and solvent removal the remaining solid was dissolved in 3 ml CH_3OH and then slowly precipitated by covering the solution with diethyl ether. The resulting final product was dried in vacuo. Yield: 71% (133 mg). $C_{31}H_{35}F_6N_6O_6RhS_3 \cdot 2H_2O$; M = 936.8 g/mol; Anal. Calc.: C, 39.7; H, 4.2; N, 9.0; S, 10.3. Found: C, 39.5; H, 4.2; N, 9.0; S, 10.3%. LSIMS: m/z 751 (22%) $[M-CF_3SO_3]^+$, 619 (44%) $[M-CF_3SO_3-\{(Me_2N)_2CS\}]^+$, 470 (100%) $[M-2CF_3SO_3-\{(Me_2N)_2CS\}]^+$. ^1H NMR (d_6-DMSO, 30 °C): δ = 1.73 (s, 15H, Cp^*-CH_3), 2.31 (s, 12H, CH_3–SC{$N(CH_3)_2$}$_2$), 8.41 (dd, 2H, H3/H8), 9.40 (s, 2H, H11/H12), 9.47 (d, 2H, H4/H7), 9.77 (d, 2H, H2/H9) ppm. ^{13}C NMR (d_6-DMSO, 30 °C): δ = 8.3 (Cp^*-C**C**H_3), 42.7 (SC{$N(\mathbf{C}H_3)_2$}$_2$),

99.4 (Cp^*-***C***CH_3), 128.5, 129.2, 136.0, 154.4 (dpq-***C***H), 138.9, 146.0, 147.0 (dpq-***C***), 179.4 (S***C***{$N(CH_3)_2$}$_2$) ppm.

4.1.7. [(η^5-C_5Me_5)Rh(dppz){SC(NMe_2)$_2$}](CF_3SO_3)$_2$ (**8**)

Preparation as for **7** with the ligands dppz (56.5 mg, 0.2 mmol) and $(Me_2N)_2CS$ (26.5 mg, 0.2 mmol). Yield: 77% (152 mg). $C_{35}H_{37}F_6N_6O_6RhS_3 \cdot 2H_2O$; M = 986.8 g/mol; Anal. Calc.: C, 42.6; H, 4.2; N, 8.5; S, 9.8. Found: C, 42.5; H, 4.3; N, 8.4; S, 10.7%. LSIMS: m/z 801 (43%) [M−CF_3SO_3]$^+$, 669 (38%) [M−CF_3SO_3−{$(Me_2N)_2CS$}]$^+$, 520 (100%) [M−2CF_3SO_3−{$(Me_2N)_2CS$}]$^+$. ^{1}H NMR (d_6-DMSO, 30 °C): δ = 1.75 (s, 15H, Cp^*-CH_3), 2.35 (s, 12H, CH_3–SC{$N(CH_3)_2$}$_2$), 8.22 (d, 2H, H12/H13), 8.42 (dd, 2H, H3/H8), 8.54 (dd, 2H, H11/H14), 9.46 (d, 2H, H4/H7), 9.87 (dd, 2H, H2/H9) ppm. ^{13}C NMR (d_6-DMSO, 30 °C): δ = 8.3 (Cp^*-C***C***H_3), 42.7 (SC{N(***C***H_3)$_2$}$_2$), 99.5 (Cp^*-***C***CH_3), 128.8, 129.4, 129.8, 139.5, 154.5 (dppz-***C***H), 132.8, 136.3, 142.1, 147.2 (dppz-***C***), 179.2 (S***C***{$N(CH_3)_2$}$_2$) ppm.

4.1.8. [(η^5-C_5Me_5)Rh(dppn){SC(NMe_2)$_2$}](CF_3SO_3)$_2$ (**9**)

Preparation as for **7** with the ligands dppn (66.5 mg, 0.2 mmol) and $(Me_2N)_2CS$ (26.5 mg, 0.2 mmol). Yield: 66% (139 mg). $C_{39}H_{39}F_6N_6O_6RhS_3 \cdot 3H_2O$; M = 1054.9 g/mol; Anal. Calc.: C, 44.4; H, 4.3; N, 8.0; S, 9.1. Found: C, 44.9; H, 4.3; N, 8.0; S, 10.4%. LSIMS: m/z 851 (47%) [M−CF_3SO_3]$^+$, 719 (48%) [M−CF_3SO_3−{$(Me_2N)_2CS$}]$^+$, 570 (100%) [M−2CF_3SO_3{$(Me_2N)_2CS$}]$^+$, ^{1}H NMR (d_6-DMSO, 30 °C): δ = 1.74 (s, 15H, Cp^*-CH_3), 2.41 (s, 12H, CH_3–SC{$N(CH_3)_2$}$_2$), 7.80 (dd, 2H, H13/H14), 8.42 (dd, 2H, H3/H8), 9.27 (s, 2H, H11/H16), 9.43 (dd, 2H, H4/H7), 9.49 (m, 2H, H12/H15), 9.85 (dd, 2H, H2/H9) ppm.

4.1.9. [(η^5-Cp^*)Rh(dppz)(C_6H_5S)](CF_3SO_3) (**10**)

Preparation as for **7** with the ligands dppz (56.5 mg, 0.2 mmol) and C_6H_5SH (20.5 μl, 0.2 mmol) and additional 37 μl 30% NaOH/CH_3OH (0.2 mmol). Yield: 86% (140 mg). $C_{35}H_{30}F_3N_4O_3RhS_2 \cdot 2H_2O$; M = 814.7 g/mol; Anal. Calc.: C, 51.6; H, 4.2; N, 6.9; S, 7.9. Found: C, 51.2; H, 4.2; N, 6.7; S, 8.0%. LSIMS: m/z 629 (82%) [M−CF_3SO_3]$^+$, 519 (100%) [M−CF_3SO_3−{C_6H_5S}]$^+$, ^{1}H NMR (d_6-DMSO, 30 °C): δ = 1.78 (s, 15H, Cp^*-CH_3), 5.83 (d, 2H, H2′/H6′), 5.90 (t,2H, H3′/H5′), 5.99 (t, 1H, H4′), 8.16 (d, 2H, H12/H13), 8.26 (dd, 2H, H3/H8), 8.47 (d, 2H, H11/H14), 9.27 (d, 2H, H4/H7), 9.57 (d, 2H, H2/H9) ppm. ^{13}C NMR (d_6-DMSO, 30 °C): δ = 8.0 (Cp^*-C***C***H_3), 97.0 (Cp^*-***C***CH_3), 129.4, 132.5, 134.2, 139.1 153.6 (dppz-***C***H), 134.4, 138.0, 141.8, 146.5 (dppz-***C***), 126.27, 126,32, 127. 70, 127.87, 128.95 (***C***H C_6H_5S), 123.92 (***C***-C_6H_5S) ppm.

4.1.10. [(η^5-C_5Me_5)Rh(dppz)($C_{10}H_7S$)](CF_3SO_3) · H_2O (**11**)

Preparation as for **7** with the ligands dppz (56.5 mg, 0.2 mmol) and $C_{10}H_7SH$ (32 mg, 0.2 mmol) and additional 37 μl 30% NaOH/CH_3OH (0.2 mmol). Yield: 67% (113 mg). $C_{39}H_{32}F_3N_4O_3RhS_2 \cdot H_2O$; M = 846.7 g/mol; Anal. Calc.: C, 55.3; H, 4.1; N, 6.6; S, 7.6. Found: C, 55.7; H, 4.0; N, 6.6; S, 7.3. LSIMS: m/z 679 (90%) [M−CF_3SO_3]$^+$, 520 (100%) [M−CF_3SO_3−{$C_{10}H_7S$}]$^+$, ^{1}H NMR (d_6-DMSO, 30 °C): δ = 1.81 (s, 15H, Cp^*-CH_3), 5.81 (s, 1H), 6.08 (d, 1H), 6.21 (m, 1H), 6.50 (m, 3H), 6.73 (d, 1H), 8.11 (d, 2H, H12/H13), 8.23 (dd, 2H, H3/H8), 8.32 (d, 2H, H11/H14), 9.29 (d, 2H, H4/H7), 9.39 (d, 2H, H2/H9) ppm. ^{13}C NMR (d_6-DMSO, 30 °C): δ = 8.1 (Cp^*-C***C***H_3), 97.2 (Cp^*-***C***CH_3), 129.5, 131.0, 132.2, 141.5, 153.6 (dppz-***C***H), 134.2, 135.6, 138.4, 146.1 (dppz-***C***), 121.1, 123.3, 123.9, 124.5, 125.2, 125.7, 127.4 (***C***H-$C_{10}H_7S$), 125.9, 128.7, 129.1 (***C***-$C_{10}H_7S$) ppm.

4.2. X-ray structural analyses

Crystals of compounds **2**–**7** and **11** suitable for X-ray structural analysis were obtained by slow evaporation of CH_3OH/H_2O solutions. Their crystal and refinement data are summarised in Table 1. Intensity data for **2**, **3** and **7** · H_2O were collected on a Siemens P4 diffractometer at 294 K using ω scans and Mo Kα radiation (λ = 0.71073 Å). An Oxford Diffraction Sapphire2 CCD diffractometer was employed for the intensity data collection of compounds **4**–**6** and **11** · $2H_2O$ using 1° ω scans and Mo Kα (for **4**, **5** and **11** · $2H_2O$) or Cu Kα radiation (for **6** = 1.54178 Å). Semi-empirical absorption corrections were applied to the intensities in all cases. The structures were solved by direct methods with SHELXS and refined against F^2 with SHELXL [46]. Anisotropic temperature factors were introduced for non-hydrogen atoms and with exception of water molecules, protons were refined at geometrically calculated positions as riding atoms. The high values of R_1 (0.122) and wR_2 (0.323) for **7** · H_2O are due to disorder of the $CF_3SO_3^-$ counter ions.

4.3. DNA binding studies

The thermal denaturation temperatures T_m of 1:10 complex/DNA mixtures [DNA concentration = M(nucleotide)] were determined for **1**–**11** in a 10 mM phosphate buffer at pH 7.2. Measurements for **10** and **11** were performed in the presence of 1% DMSO. Melting curves were recorded at 1° steps for the wavelength λ = 260 nm with an analytikjena SPECORD 200 spectrometer equipped with a Peltier temperature controller. T_m values were calculated by determining the midpoints of melting curves from the first order derivatives. The experimental ΔT_m values are estimated to be accurate within ±1 °C. Concentrations of CT DNA were determined spectrophotometrically using the molar extinction coefficient ε_{260} = 6600 M^{-1} cm^{-1} [47].

Viscosities for mixtures of complexes **1**–**9** with sonicated DNA were determined using a Cannon-Ubbelhode semi-micro dilution viscometer (Series No. 75, Cannon Instruments Co.) held at a constant temperature of 25 °C in a water bath. The viscometer initially contained 2 ml of 0.4 mM sonicated DNA solution in a 10 mM phosphate buffer (pH 7.2). 0.2 mM complex solutions also containing 0.4 mM sonicated DNA were added in increments of 100 μl from a micropipet. Solutions were passed through filters to remove particulate material prior to use. Reduced viscosities η were calculated by literature methods [32] and plotted as $\ln(\eta/\eta_o)$ (η_o = reduced viscosity of the DNA solution in the absence of complex) against $\ln(1 + r)$ for rod-like DNA (approximately 600 base pairs).

4.4. Cell cultures

MCF-7 breast cancer and HT-29 human colon carcinoma cells were maintained in 10% (v/v) fetal calf serum containing cell culture medium (minimum essential medium eagle supplemented with 2.2 g $NaHCO_3$, 110 mg l^{-1} sodium pyruvate and 50 mg l^{-1} gentamicin sulfate adjusted to pH 7.4) at 37 °C: 5% CO_2 and passaged twice a week according to standard procedures.

4.5. Cellular uptake studies

For cellular uptake studies, HT-29 and MCF-7 cells were grown until at least 70% confluency in 175 cm^2 cell culture flasks. Stock solutions of complexes **1**–**11** in DMSO were freshly prepared and diluted with cell culture medium to the desired concentrations (final DMSO concentrations: 0.1% v/v, final complex concentration: 1.0–100 μM). The cell culture medium of the cell culture flasks was replaced with 10 ml of the cell culture medium solutions containing **1**–**11** and the flasks were incubated for 6 h at 37C/5% CO_2 The cell pellets were isolated, resuspended in 1–5 ml twice distilled water, lysed by using a sonotrode and appropriately diluted using twice distilled water. The rhodium content of the samples was determined by atomic absorption spectroscopy (AAS, see below) and the protein content of separate aliquots by the Bradford method. To correct for matrix effects in AAS measurements, samples and standards were adjusted to the same protein concentration by dilution with twice distilled water (matrix matched

Table 5
Graphite furnace program for AAS measurements

Step	Temperature (°C)	Ramp (°C/s)	Hold (s)
Drying	90	10	40
Drying	105	7	30
Drying	120	15	20
Drying	500	50	30
Pyrolysis	1200	200	20
AZ(zeroing)	1200	0	6
Atomisation	2400	Maximum	9
Tube cleaning	2500	1000	6

calibration). Prior to AAS analysis 20 μl Triton X-100 (1%) and 20 μl nitric acid acid (13%) were added to each 200 μl sample of the cell suspensions. Cellular uptake was expressed as ng rhodium per mg cell protein for data obtained from two independent experiments.

4.6. Atomic absorption spectroscopy

A Vario 6 graphite furnace atomic absorption spectrometer (Analytik Jena) was employed for the Rh quantification using a wavelength of 343.5 nm with a bandpass of 0.5 nm. A deuterium lamp was used for background correction. Matrix containing standards were obtained by addition of a rhodium stock solution (1 mg/mL Rh in 10% HCl) to untreated cell suspensions. Probes were injected at a volume of 20 μl into standard graphite tubes. Drying, pyrolysis and atomization in the graphite furnace were performed according to the conditions listed in Table 5. During the temperature program the graphite tube was purged with a constant argon gas flow, which was only halted during the zeroing and atomisation steps. Pyrolysis and atomisation temperatures were optimised prior to the experiments. The recovery rates of the metallodrugs were determined initially and used for calculation of the final experimental values. The mean integrated absorbances of duplicate injections were used throughout the study. The characteristical concentration for the described method was $0.85^{\pm 0.05}$ (μg Rh l^{-1})/1% A.

4.7. Cytotoxicity measurements

The antiproliferative effects of the compounds were determined following an established procedure [48]. Cells were suspended in cell culture medium (HT-29: 2850 cells/ml, MCF-7: 10^5 cells/ml), and 100 μl aliquots thereof were plated in 96 well plates and incubated at 37 °C: 5% CO_2 for 48 h (HT-29) or 72 h (MCF-7). Stock solutions of the compounds in DMSO were freshly prepared and diluted with cell culture medium to the desired concentrations (final DMSO concentration: 0.1% v/v). The medium in the plates was replaced with medium containing the compounds in graded concentrations (six replicates). After further incubation for 72 h (HT-29) or 96 h (MCF-7) the cell biomass was determined by crystal violet staining and the IC_{50} values were established as those concentrations causing 50% inhibition of cell proliferation. Results were calculated from 2 to 3 independent experiments.

Acknowledgements

Financial support of this work in Bochum and Berlin by the Deutsche Forschungsgemeinschaft (DFG) within the research group FOR 630 "Biological function of Organometallic Compounds" is gratefully acknowledged. We are also grateful to Heike Mayer-Figge and Heike Scheffler for technical support.

Appendix A. Supplementary material

CCDC 675527, 675528, 675529, 675530, 675531, 675532 and 675533 contain the supplementary crystallographic data for this paper. These data can be obtained free of charge from The Cambridge Crystallographic Data Centre via www.ccdc.cam.ac.uk/data_request/cif. Supplementary data associated with this article can be found, in the online version, at doi:10.1016/j.jorganchem.2008.04.002.

References

[1] E. Hillard, A. Vessières, F. Le Bideau, D. Plazuk, D. Spera, M. Huche, G. Jaouen, ChemMedChem 1 (2006) 551.
[2] A. Habtemariam, M. Melchart, R. Fernandez, S. Parsons, I.D.H. Oswald, A. Parkin, F.P.A. Fabbiani, J.E. Davidson, A. Dawson, R.E. Aird, D.I. Jodrell, P.J. Sadler, J. Med. Chem. 49 (2006) 6858.
[3] P.J. Dyson, G. Sava, Dalton Trans. (2006) 1929.
[4] A. Vessières, S. Top, W. Beck, E. Hillard, G. Jaouen, Dalton Trans. (2006) 529.
[5] L. Dale, J.H. Tocher, T.M. Dyson, D.I. Edwards, D.A. Tocher, Anti-Cancer Drug Des. 7 (1992) 3.
[6] Y.N. Vashisht Gopal, D. Jayaraju, A.K. Kandapi, Biochemistry 38 (1999) 4382.
[7] Y.N. Vashisht Gopal, N. Konura, A.K. Kandapi, Arch. Biochem. Biophys. 401 (2002) 53.
[8] L.A. Huxham, E.L.S. Cheu, B.O. Patrick, B.R. James, Inorg. Chim. Acta 352 (2003) 238.
[9] C.S. Allardyce, P.J. Dyson, D.J. Ellis, S.L. Heath, Chem. Commun. (2001) 1396.
[10] W.S. Sheldrick, S. Heeb, Inorg. Chim. Acta 168 (1990) 93.
[11] R.E. Morris, R.E. Aird, P.delS. Murdoch, H.M. Chen, J. Cummings, N.D. Hughes, S. Parsons, A. Parkin, G. Boyd, D.I. Jodrell, P.J. Sadler, J. Med. Chem. 44 (2001) 3616.
[12] A.F.A. Peacock, A. Habtemariam, R. Fernández, V. Walland, F.P.A. Fabbiani, S. Parsons, R.E. Aird, D.J. Jodrell, P.J. Sadler, J. Am. Chem. Soc. 128 (2006) 1739.
[13] A.F.A. Peacock, A. Habtemariam, S.A. Moggach, A. Prescimone, S. Parsons, P.J. Sadler, Inorg. Chem. 46 (2007) 4049.
[14] A. Dorcier, W.H. Ang, S. Bolaño, L. Gonsalvi, L. Juillerat-Jeannerat, G. Laurenczy, M. Peruzzini, A.D. Phillips, F. Zanobini, P.J. Dyson, Organometallics 25 (2006) 4090.
[15] S. Schäfer, I. Ott, R. Gust, W.S. Sheldrick, Eur. J. Inorg. Chem. (2007) 3034.
[16] K.E. Erkkila, D.T. Odom, J.K. Barton, Chem. Rev. 99 (1999) 2777.
[17] C. Metcalfe, J.A. Thomas, Chem. Soc. Rev. 32 (2003) 215.
[18] E.L. Menon, R. Perera, M. Navarro, R.J. Kuhn, H. Morrison, Inorg. Chem. 43 (2004) 5373.
[19] S. Schäfer, W.S. Sheldrick, J. Organomet. Chem. 692 (2007) 1300.
[20] L. Dadci, H. Elias, U. Frey, A. Hörnig, U. Koelle, A.F. Merbach, H. Paulus, J.S. Schneider, Inorg. Chem. 34 (1995) 306.
[21] D.A. Herebian, C.S. Schmidt, W.S. Sheldrick, C. van Wüllen, Eur. J. Inorg. Chem. (1998) 1991.
[22] G. Garcia, G. Sánchez, I. Romero, I. Solano, M.D. Santana, G. Lopez, J. Organomet. Chem. 408 (1991) 241.
[23] U. Kölle, M. Grätzel, Angew. Chem., Int. Ed. Engl. 26 (1987) 507.
[24] U. Kölle, B.-S. Kang, P. Infelta, P. Comte, M. Grätzel, Chem. Ber. 122 (1989) 1869.
[25] M.-T. Youinou, R. Ziessel, J. Organomet. Chem. 363 (1989) 197.
[26] S. Berger, J. Fiedler, R. Reinhardt, W. Kaim, Inorg. Chem. 43 (2004) 1530.
[27] D.A. Herebian, W.S. Sheldrick, J. Chem. Soc., Dalton Trans. (2002) 966.
[28] A. Frodl, D. Herebian, W.S. Sheldrick, J. Chem. Soc., Dalton Trans. (2002) 3664.
[29] S. Gençaslan, W.S. Sheldrick, Eur. J. Inorg. Chem. Soc. (2005) 3840.
[30] D.M. Gray, in: G.D. Fasman (Ed.), Circular Dichroism and the Conformational Analysis of Biomolecules, Plenum Press, New York, 1996, p. 469.
[31] W.C. Johnson, in: N. Berova, K. Nakanishi, R.W. Woody (Eds.), Circular Dichroism: Principles and Applications, 2nd ed., VCH Publishers, New York, 2000, p. 523.
[32] G. Cohen, H. Eisenberg, Biopolymers 4 (1966) 429.
[33] D. Suh, J.B. Chaires, Bioorg. Med. Chem. 3 (1995) 723.
[34] K.K.-W. Lo, C.-K. Chung, N. Zhu, Chem. Eur. J. 12 (2006) 1500.
[35] V.W.-W. Yam, K.K.-W. Lo, K.-K. Cheung, R.Y.-C. Kong, J. Chem. Soc., Dalton Trans. (1997) 2067.
[36] K.K.-W. Lo, R.Y.-C. Kong, Organometallics 23 (2004) 3062.
[37] S.P. Foxon, C. Metcalfe, H. Adams, M. Webb, J.A. Thomas, Inorg. Chem. 46 (2007) 409.
[38] J. Sartorius, H.-J. Schneider, J. Chem. Soc., Perkin Trans. 2 (1997) 2319.
[39] A. Raja, V. Rajendrian, P. Uma Masheswari, R. Balamunrugam, C.A. Kilner, M.A. Halcrow, M. Palaniandavar, J. Inorg. Biochem. 99 (2005) 1717.
[40] B. Selvakumar, V. Rajendrian, P. Uma Masheswari, H. Stoecki-Evans, M. Palaniandavar, J. Inorg. Biochem. 100 (2006) 316.
[41] M. Scharwitz, I. Ott, R. Gust, A. Kromm, W.S. Sheldrick, J. Inorg. Biochem. (2008), doi:10.1016/j.jinorgbio.2008.03.001.
[42] J.S. Ren, T.C. Jenkins, J.B. Chaires, Biochemistry 39 (2000) 8439.
[43] J.W. Kang, K. Moseley, P.M. Maitlis, J. Am. Chem. Soc. 91 (1969) 5970.
[44] J.G. Collins, A.D. Sleemann, J.R. Aldrich-Wright, I. Greguric, T.W. Hambley, Inorg. Chem. 37 (1998) 3133.
[45] A. Delgadillo, P. Romo, A.M. Leiva, B. Loeb, Helv. Chim. Acta 86 (2003) 2110.
[46] G.M. Sheldrick, SHELXS97 and SHELXL 97, Göttingen, Germany, 1997.
[47] J. Marmur, J. Mol. Biol. 3 (1961) 208.
[48] I. Ott, K. Schmidt, B. Kircher, P. Schuhmacher, T. Wiglenda, R. Gust, J. Med. Chem. 48 (2005) 622.